

# Analysis of strong scattering at the micro-scale

Kasper van Wijk<sup>1</sup>, Dimitri Komatitsch<sup>2</sup>, John A. Scales<sup>1</sup> and Jeroen Tromp<sup>2</sup>

<sup>1</sup>*Physical Acoustics Laboratory and Center for Wave Phenomena, Colorado School of Mines*

<sup>2</sup>*Seismological Laboratory, California Institute of Technology*

## ABSTRACT

Exploiting the fine structure of strongly scattered surface waves could provide a wealth of new information in seismology, ultrasonics, acoustics and other fields that study wave propagation in highly heterogeneous media. Toward this end, we have made laboratory measurements of ultrasonic waves propagating in disordered media. Spectral-element simulations of these models provide us with a powerful tool for understanding the complex dynamics of diffraction and scattering; issues that need to be addressed in seismic hazard studies in global seismology and static corrections for exploration geophysics. This paper focuses on small-scale scattering, such as diffracted body waves, which are weak precursors to the dominant surface waves; these events may be analogous to diffractions from the Earth’s rough core-mantle boundary.

## INTRODUCTION

Indications of multiple scattering in seismic waves have been observed (Aki & Chouet, 1975; Campillo & Paul, 2003; Hennino *et al.*, 2001), but questions remain as to how to characterize media in which energy is multiply scattered. In the Physical Acoustics Laboratory, we study wave propagation in strongly heterogeneous media such as rocks and engineered materials. In previous work we have described what we call a “tunable” multiple scattering system, consisting of a block of aluminum with a disordered pattern of grooves cut in it (Scales & van Wijk, 1999; Scales & van Wijk, 2001). Surface waves propagating parallel to the grooves are not scattered, while waves propagating normal to the grooves are so strongly scattered that the behavior rapidly becomes diffusive. Bulk properties of the propagation, including attenuation and dispersion, were studied to describe the scattering model on the macroscopic scale, while in (van Wijk *et al.*, 2003) we used a radiative transfer model to study the mesoscopic scale of the medium in terms of scattering and absorption mean free paths.

Quantifying the results of surface-wave scattering from lateral variations is of direct interest in geophysics. Scattering caused by topographic variations introduces dispersion of the early arriving energy, which competes with dispersion related to horizontally layered structures. In addition, in global seismology, surface topography or sedimentary basins can trap seismic energy, posing seismic hazard, while in exploration geophysics topography needs to be accounted for in terms of static corrections (Campman *et al.*, 2003).

Here, we introduce two-dimensional (2D) numerical simulations of the physical system, using the spectral-element method (SEM) (Komatitsch & Tromp, 1999) to model the ultrasonic experiment with sharp topographic features, and investigate subtle details in the laboratory data, on the scale of the individual scatterer, i.e. the microscopic scale. Henceforth, we refer to the vertical component of the particle velocity measured in laboratory experiments as “data” and to the numerical results as “simulations.”

## 1 PHYSICAL EXPERIMENT

The setup of the experiment is shown in Figure 1. A 200 V repetitive pulse is used to excite an angle-beam transducer mounted on the surface of an aluminum block of dimensions 280 mm × 230 mm × 215 mm. The transducer wedge has a footprint of 70 mm by 42 mm. The angle of the transducer is such that its output in the aluminum block is mainly a surface (Rayleigh) wave with a dominant wavelength around 10 mm. The source wavelet is planar over the width of the transducer, making our model 2D. The wave field is detected by a scanning laser vibrometer that measures absolute particle velocity on the surface of the sample via the Doppler shift. The signal is digitized at 14-bit resolution using a Gage digital oscilloscope card. The entire setup is positioned on a vibration isolation table to reduce background noise.

The aluminum block has a Fibonacci pattern of

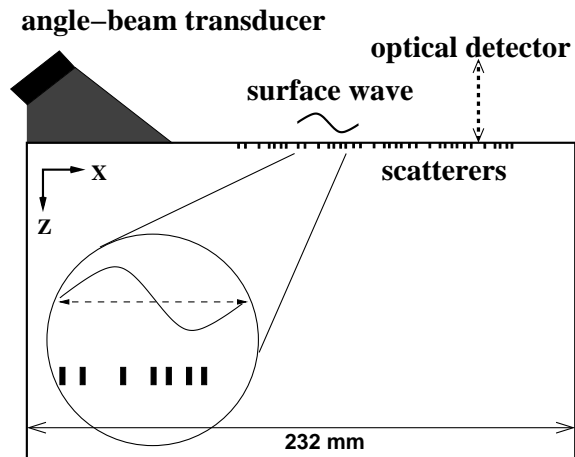


**Figure 1.** Schematic setup of the experiment. The angle-beam transducer generates a Rayleigh wave that is multiply scattered by the grooves cut into the aluminum model. Vertical particle velocity is recorded by the laser Doppler vibrometer.

aligned linear grooves machined into one face. This sequence is quasi-periodic, but increases in complexity as it gets longer (Carpena *et al.*, 1995). The grooves are nominally 1 mm wide, 2.75 mm deep and 1 or 2 mm apart, but to represent the actual groove pattern as accurately as possible in the numerical model, we scanned the surface at 2400 dots per inch, allowing us to include variations in the widths of the grooves and the surface between grooves, which we call a non-groove.

## 2 NUMERICAL MODELING

A 2D version of the spectral-element method (SEM), mostly used and validated in seismology (Priolo *et al.*, 1994; Faccioli *et al.*, 1997; Komatitsch & Vilotte, 1998; Komatitsch & Tromp, 1999; Komatitsch & Tromp, 2002; Komatitsch *et al.*, 2002), is used to simulate wave propagation at ultrasonic frequencies in a model that contains a large number of sharp grooves. The SEM is ideal for this purpose because we can use its flexibility to mesh the grooved structure based on a geometrically non-conforming mesh and also because it has been shown to be accurate in modeling surface waves (Komatitsch & Tromp, 1999). The simulations can be compared to measurements at every surface location, because the optical detector can record at any location on the surface of the block (Figure 1). The source in the simulations is the analytic solution to a Rayleigh wave (Komatitsch *et al.*, 1999) and detectors are located in a line directly in front of the source. Attenuation is so weak in aluminum that elastic simulations are meaningful.

Near the surface, the block is modeled by a mesh

with cells whose size is on the order of a scatterer, but the mesh size is doubled twice with depth to reduce the total number of cells (i.e., spectral elements) to 11426. We use a polynomial of degree  $N=4$  to interpolate the wave field in each quadrangular cell; the total number of grid points is 184141. The time step used in the explicit integration scheme is  $\Delta t = 10^{-5}$  ms and we propagate the signal for 0.2 ms.

## 3 COMPARING DATA AND SIMULATIONS

We compare data and simulations at 20 detector locations at 5 mm increments on the smooth face of the model, and on the first 42 non-grooves along a line perpendicular to the grooves (strong scattering). In both experiments, the source-detector offset for the first trace is 2 mm.

The data and simulations on the smooth aluminum surface are shown in Figure 2. Both panels show a large direct surface-wave arrival, followed by a reflection from the far end of the aluminum block. The wavelet in the data has some energy after the main pulse caused by ringing in the transducer. This energy is not included in the source term of the simulations. The data show little attenuation and no evidence of reflections from the sides of the block, which means that the source energy emitted has little geometrical spreading, justifying 2D elastic simulations.

Figure 3 shows the data (left) and simulations (right) for waveforms in the strong scattering case. At each groove, energy is partially reflected, causing the direct arrival to be attenuated and the group velocity to be lowered, compared to the un-scattered wave propagation. This strong scattering has been shown to lead to diffusive behavior of energy propagation (Scales & van Wijk, 2001). The strongest events are interfering surface waves, which look qualitatively similar in the two panels. These strong events show coherence in the sense that a single phase can be tracked from one detector location to the next, whereas for late times, scattering causes arrivals to be incoherent from trace to trace. In general, detailed differences between the numerical mesh and the grooved block are amplified at later times as a result of multiple scattering, much as in coda wave interferometry (Snieder *et al.*, 2002): waves bouncing back-and-forth numerous times between scatterers highlight errors in the numerical representation. The later events especially show greater discrepancy in amplitude, because the path-lengths for the multiply scattered events are longer than the early arrivals, so that neglecting attenuation in aluminum becomes a significant source for the difference between data and simulations.

The amplitude of the maximum correlation between data and simulations directly reflects the accuracy of the simulations: correlation of unity means that data and simulations are identical. It is our experience

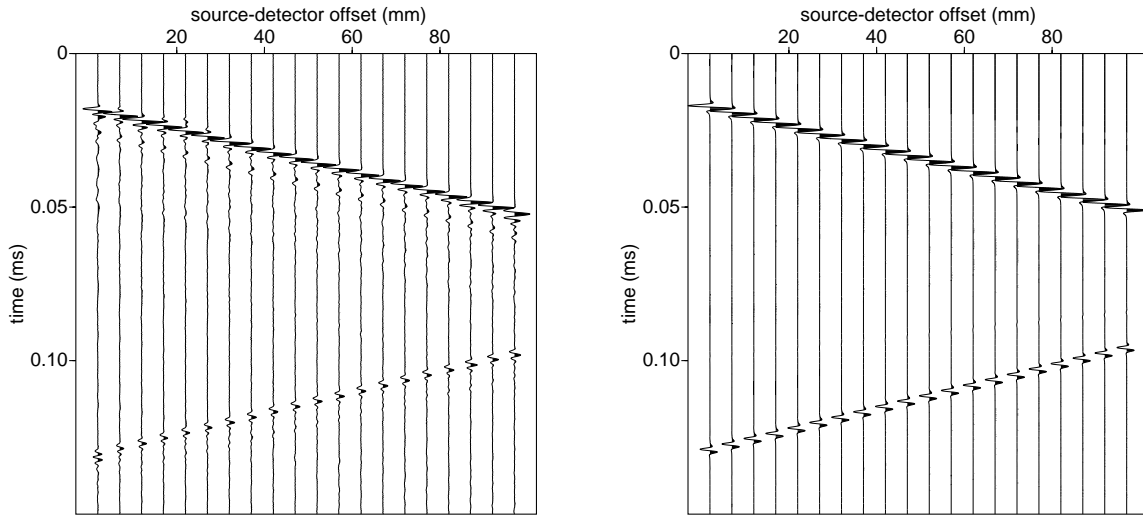


Figure 2. Data (left) and simulations (right) for wave paths on the smooth side of the model.

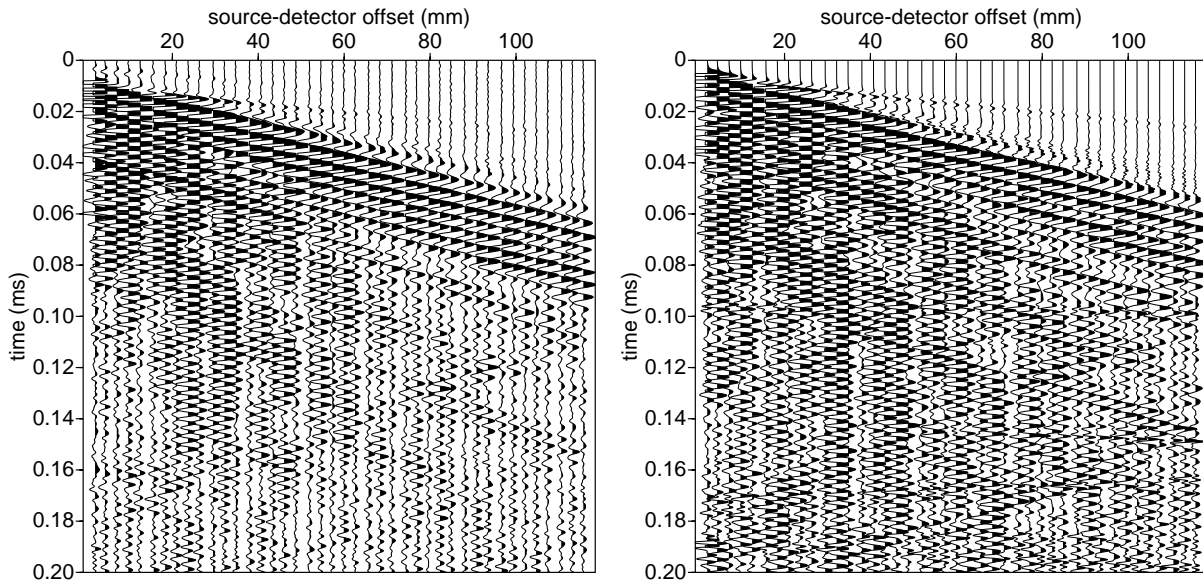
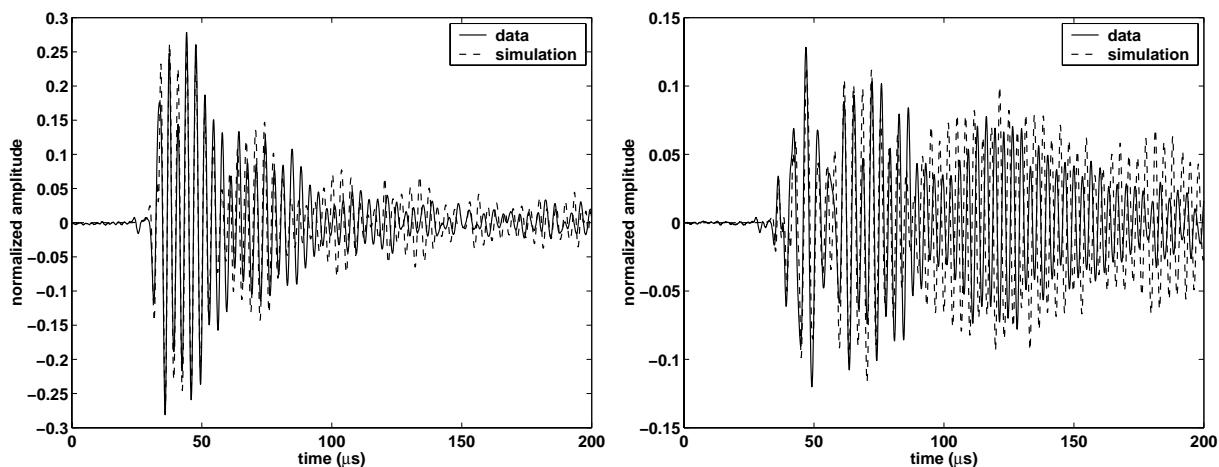


Figure 3. Data (left) and simulations (right) for wave paths on the grooved side of the model. The main energy consists of surface waves bouncing between grooves, but the small-amplitude, faster events are body-waves diffracted at the grooves.

that discrepancies between the physical and numerical models on the order of a fraction of the size of a single scatterer have a noticeable influence on the accuracy of the simulations.

The maximum cross-correlation for the case of strong scattering is overall lower than for the experiment on the smooth side (Figure 4). Especially for source-detector distances greater than 90 mm, small discrepancies between the physical model and numerical repre-

sentation get amplified. However, the simulations are of such precision that both data and simulations on a non-groove with the size on the order of 1 mm show considerably more energy at later times than do traces on the thicker non-grooves. An example of this is detector 12, compared to detector 4 (Figure 5): the relatively thin ridge of aluminum under detector 12 is excited in a 300-kHz resonance. While this mode is too low in frequency to represent a trapping of energy in the non-groove, it



**Figure 5.** Comparison between data and simulations for detector 4 (left) and 12 (right) on the grooved side of the model. Note the relatively stronger amplitudes at later times for detector 12.

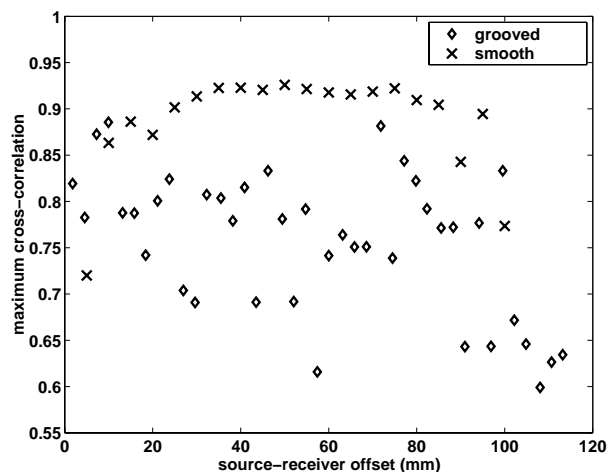


**Figure 4.** Maximum correlation between data and simulations, both on the smooth side and the grooved side of the model. Identical traces have correlation 1.

is possible that this resonance is a flexural mode of the thin non-groove (Rossing & Fletcher, 1995).

Also, we noted that the source wedge acts as an additional scatterer in the model, causing the maximum correlation on the smooth side of the aluminum to be smallest for detector 1 (Figure 4). Note the differences in amplitude and phase in the direct arrival and more clearly in the reflected event (Figure 6), when compared to the other traces in Figure 2. This is due to the influence of the source wedge, which is located only 2 mm from detector 1. The second reflection from the edge of the block near the source is almost undetected in the data, because it requires the Rayleigh wave to travel along the surface between the bottom of the source wedge and the aluminum block. This is not an obsta-

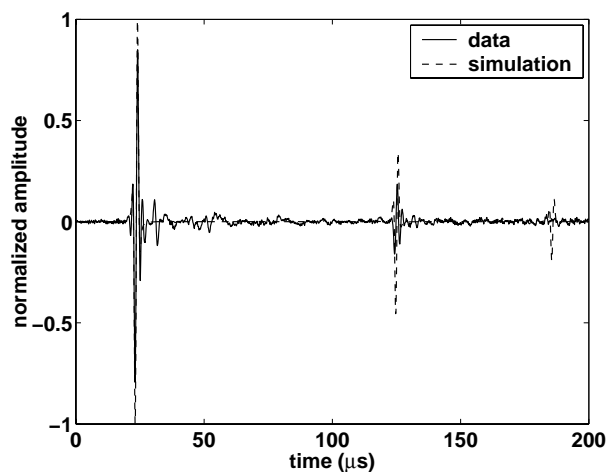


**Figure 6.** Comparison between data and simulations for detector 1 on the smooth side of the model.

cle in the simulations, because the source is modeled by an analytically incident Rayleigh wave. A completely non-contacting experimental setup with a laser source in addition to the optical detector (Scales & Malcolm, 2003) would be ideal, but for this application the laser source is too high in frequency for energy to penetrate the groove sequence significantly.

#### 4 PRECURSORS

In the strong-scattering case, relatively lower-amplitude and faster events arrive before the main surface-wave energy (Figure 3). The data panel shows two coherent events with the P-wave velocity of aluminum. The first, starting at  $t=0$ , is caused by the angle-beam transducer



**Figure 7.** Experimental configuration, where the source is perpendicular to a single groove on the top of the block, while the detector scans the side.

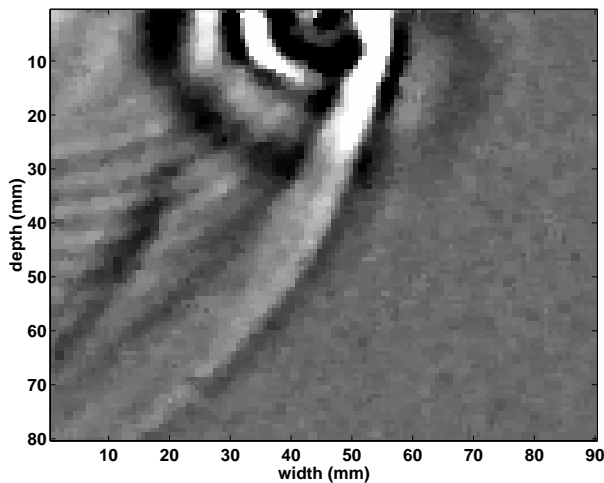


**Figure 8.** Snap-shot of particle motion in the scanned region after the incident field scattered off a single groove.

producing some P-waves in addition to surface-wave energy. This event is not present in the simulations, because the source is a pure Rayleigh wave. The second event with a P-wave velocity cannot be seen until the 6th or 7th trace at  $t = 0.01$  ms, but is confirmed by the simulations. These events are spherical body-wave fronts diffracted at the individual grooves, which arrive before the Rayleigh waves, and may be analogous to precursors to the seismic phase PKKP in global seismology, believed to be caused by scattering at the rough boundary between the Earth's outer-core and mantle (Earle & Shearer, 1997).

To support the existence of body-wave precursors to the surface-wave energy, we conducted a second experiment, where the source is mounted on the face of the aluminum model with a single groove, while the detector

scans the side of the model (Figure 7). Figure 8 shows a snap-shot of particle motion, measured shortly after the incident wave interacted with the single groove. The side of the aluminum block breaks the symmetry of the Rayleigh-wave motion purely in the  $x$ - and  $z$ -direction, creating particle motion in the  $y$ -direction. Higher frequencies in the upper left part are due to ringing of the source, and the incident field is the strong event extending from top to bottom. The circular events are body-waves scattered off the single groove. Scattering to body waves is stronger in the backward direction, but significant P-wave energy travels ahead of the surface wave, causing the precursors observed in Figure 3.

## 5 CONCLUSIONS

In the Physical Acoustics Laboratory, we study phenomena that arise from multiply scattered surface waves on a physical system in which we can measure the wave-forms between scatterers. In general, surface topography causes scattering of seismic energy, leading to attenuation and dispersion. Here, we analyzed relatively small-amplitude features from individual scatterers, confirmed by spectral-element simulations. For example, body-wave precursors to the main surface-wave energy are caused by diffraction from the scatterers, which may be analogous to PKKP precursors, believed to be caused by scattering at the rough core-mantle boundary.

## ACKNOWLEDGMENTS

This work was supported by The National Science Foundation (EAR-0111804 and EAR-0003761) and the Army Research Office (DAAG55-98-1-0277). We acknowledge Francisco Sánchez-Sesma for the use of his Rayleigh wave code, and Roel Snieder and Ken Larner for stimulating discussions. This is contribution No. 8928 of the Division of Geological and Planetary Sciences of the California Institute of Technology.

## REFERENCES

- Aki, K., & Chouet, B. 1975. Origin of coda waves: source, attenuation and scattering effects. *Journal of Geophysical Research*, **80**, 3322–3342.
- Campillo, M., & Paul, A. 2003. Long-range correlations in the diffuse seismic coda. *Science*, **299**, 547–549.
- Campman, X. H., van Wijk, K., Scales, J. A., & Herman, G. C. 2003. Suppression of near-field scattered surface waves. *In: Extended Abstracts, 65th Mtg. Eur. Assn. Geosci. Eng.*
- Carpena, P., Gasparian, V., & Ortuño, M. 1995. Energy spectra and level statistics of Fibonacci and Thue-Morse chains. *Physical Review B*, **51**(18), 12813–12816.
- Earle, P. S., & Shearer, P. M. 1997. Observations of PKKP precursors used to estimate small-scale topography on the core-mantle boundary. *Science*, **277**, 667–670.

- Faccioli, E., Maggio, F., Paolucci, R., & Quarteroni, A. 1997. 2D and 3D elastic wave propagation by a pseudo-spectral domain decomposition method. *J. Seismol.*, **1**, 237–251.
- Hennino, R., Trégourès, N., Shapiro, N. M., L. Margerin, L., Campillo, M., Tiggelen, B. A. Van, & Weaver, R. L. 2001. Observation of equipartition of seismic waves. *Physical Review Letters*, **86**(15), 3447–3450.
- Komatitsch, D., & Tromp, J. 1999. Introduction to the spectral-element method for 3-D seismic wave propagation. *Geophys. J. Int.*, **139**, 806–822.
- Komatitsch, D., & Tromp, J. 2002. Spectral-element simulations of global seismic wave propagation-I. Validation. *Geophysical Journal International*, **150**, 390–412.
- Komatitsch, D., & Vilotte, J. P. 1998. The spectral-element method: an efficient tool to simulate the seismic response of 2D and 3D geological structures. *Bull. Seism. Soc. Am.*, **88**, 368–392.
- Komatitsch, D., Vilotte, J. P., Vai, R., Castillo-Covarrubias, J. M., & Sánchez-Sesma, F. J. 1999. The spectral element method for elastic wave equations— application to 2-D and 3-D seismic problems. *International Journal for Numerical Methods in Engineering*, **45**, 1139–1164.
- Komatitsch, D., Ritsema, J., & Tromp, J. 2002. The spectral-element method, Beowulf computing, and global seismology. *Science*, **298**, 1737–1742.
- Priolo, E., Carcione, J. M., & Seriani, G. 1994. Numerical simulations of interface waves by high-order spectral modeling techniques. *J. Acoust. Soc. Am.*, **95**, 681–693.
- Rossing, T. D., & Fletcher, N. H. 1995. *Principles of vibration and sound*. Springer-Verlag.
- Scales, J. A., & Malcolm, A. E. 2003 (April). *Laser characterization of ultrasonic wave propagation in random media*. To appear in *Phys. Rev. E*.
- Scales, J. A., & van Wijk, K. 1999. Multiple scattering attenuation and anisotropy of ultrasonic surface waves. *Applied Physics Letters*, **74**, 3899–3901.
- Scales, J. A., & van Wijk, K. 2001. Tunable multiple-scattering system. *Applied Physics Letters*, **79**, 2294–2296.
- Snieder, R., Grêt, A., Douma, H., & Scales, J. A. 2002. Coda Wave Interferometry for Estimating Nonlinear Behavior in Seismic Velocity. *Science*, **295**, 2253–2255.
- van Wijk, K., Haney, M., & Scales, J. A. 2003. *Energy propagation in a 1D attenuative medium in the laboratory*. CWP Project Review.